APL Materials

Defects at the surface of β-Ga_2O_3 produced by Ar plasma exposure

Cite as: APL Mater. **7**, 061102 (2019); https://doi.org/10.1063/1.5109025
Submitted: 05 May 2019 . Accepted: 29 May 2019 . Published Online: 18 June 2019

A. Y. Polyakov, In-Hwan Lee, N. B. Smirnov, E. B. Yakimov, I. V. Shchemerov, A. V. Chernykh, A. I. Kochkova, A. A. Vasilev, P. H. Carey, F. Ren, David J. Smith, and S. J. Pearton

View Online Export Citation CrossMark

ARTICLES YOU MAY BE INTERESTED IN

A review of Ga_2O_3 materials, processing, and devices
Applied Physics Reviews **5**, 011301 (2018); https://doi.org/10.1063/1.5006941

Large-area MoS_2-MoO_x heterojunction thin-film photodetectors with wide spectral range and enhanced photoresponse
APL Materials **7**, 061101 (2019); https://doi.org/10.1063/1.5094586

Anisotropic etching of β-Ga_2O_3 using hot phosphoric acid
Applied Physics Letters **115**, 013501 (2019); https://doi.org/10.1063/1.5093188

AMERICAN ELEMENTS
THE ADVANCED MATERIALS MANUFACTURER®

American Elements opens up a world of possibilities so you can **Now Invent!**

Over 15,000 certified high purity laboratory chemicals, metals, & advanced materials and a state-of-the-art Research Center. Printable GHS-compliant Safety Data Sheets. Thousands of new products. And much more. All on a secure multi-language "Mobile Responsive" platform.

Now Invent.™
The Next Generation of Material Science Catalogs
www.americanelements.com

© 2019 Author(s).

Defects at the surface of β-Ga_2O_3 produced by Ar plasma exposure

Cite as: APL Mater. 7, 061102 (2019); doi: 10.1063/1.5109025
Submitted: 5 May 2019 • Accepted: 29 May 2019 •
Published Online: 18 June 2019

View Online Export Citation CrossMark

A. Y. Polyakov,[1] In-Hwan Lee,[2] N. B. Smirnov,[1] E. B. Yakimov,[1,3] I. V. Shchemerov,[1] A. V. Chernykh,[1] A. I. Kochkova,[1] A. A. Vasilev,[1] P. H. Carey,[4] F. Ren,[4] David J. Smith,[5] and S. J. Pearton[6]

AFFILIATIONS

[1]National University of Science and Technology MISiS, 4 Leninskiy Ave., Moscow 119049, Russia
[2]Department of Materials Science and Engineering, Korea University, Seoul 02841, South Korea
[3]Institute of Microelectronics Technology and High Purity Materials, Russian Academy of Science, 6 Academician Ossipyan Str., Chernogolovka, Moscow Region 142432, Russia
[4]Department of Chemical Engineering, University of Florida, Gainesville, Florida 32611, USA
[5]Department of Physics, Arizona State University, Tempe, Arizona 85287, USA
[6]Department of Materials Science and Engineering, University of Florida, Gainesville, Florida 32611, USA

ABSTRACT

Films of β-Ga_2O_3 grown by halide vapor phase epitaxy on native substrates were subjected to Ar inductively coupled plasma treatment. As a result, the built-in voltage of Ni Schottky diodes deposited on the plasma treated surfaces decreased from 1 V to −0.02 V due to the buildup of deep trap concentration in the near surface region. Deep level spectra measurements indicate a strong increase in the top ~200 nm of the plasma treated layer of the concentration of $E2^*$ (Ec − 0.8 eV) and especially E3 (Ec − 1.05 eV) deep electron traps. Capacitance-voltage profiling with monochromatic illumination also indicated a large increase in the upper ~100 nm of the film in the concentration of deep acceptors with optical threshold for an ionization of ~2.3 eV and 3.1 eV. Such defects at the surface led to a significant increase in reverse current, an increase in the ideality factor in forward current, and a dramatic decrease in the diffusion length of nonequilibrium charge carriers from 450 nm to 150 nm.

© 2019 Author(s). All article content, except where otherwise noted, is licensed under a Creative Commons Attribution (CC BY) license (http://creativecommons.org/licenses/by/4.0/). https://doi.org/10.1063/1.5109025

INTRODUCTION

The β-polytype of Ga_2O_3 is emerging as a potential candidate for next generation high-power/high-temperature devices and solar-blind UV photodetectors.[1–11] The excellent intrinsic properties of this material include a wide bandgap of ~4.8 eV, a high electrical breakdown field of ~8 MV/cm, and a high electron saturation velocity of ~10^7 cm/s.[1–8] Combined with availability of excellent crystalline quality native substrates prepared by solution growth techniques,[1] high quality epitaxial films, and existence of wide-bandgap ternaries of $(Al_xGa_{1-x})_2O_3$ that can be used as barrier layers in modulation doped field effect transistors (MODFETs),[1,12] there is clearly a basis for optimism about the technological prospects. In addition, efficient donor doping is available in bulk and epi growth methods, and it is possible to grow semi-insulating buffer layers for lateral transistors.[1–6] It is difficult to wet etch high quality Ga_2O_3,[13] and for device patterning for isolation, it is usual to employ dry etching using chlorine-based chemistries, especially BCl_3/Ar gas mixtures.[14–19] Since Ga_2O_3 has a high bond strength, Ar provides an enhanced physical component to the etching and is needed to help break bonds and facilitate formation of volatile $GaCl_x$ and O_2 etch products.[19] A concern is that such plasma treatment regimes, providing practical and controlled etch rates and good selectivity, also tend to introduce surface damage, leading to increased leakage, lower breakdown voltages, and ideality factors in forward current considerably higher than unity.[14,15]

Previous studies have shown that the Ga_2O_3 surface is sensitive to damage during plasma exposure under high ion density conditions, leading to the introduction of generation-recombination centers that degrade the Schottky characteristics.[14,15,20] These are most

© Author(s) 2019

likely related to Ga vacancies.[21] This damage is partially recovered by 500 °C annealing.[14,15] Moreover, there are also chemical effects that may alter the surface properties,[1,4,22–24] such as the presence of hydrogen in O–H groups that dramatically alter the surface accumulation or depletion of electrons.[23] Thermal cleaning by high temperature anneals in high vacuum at 800 °C was able to shift the band-bending by as much as 0.5 eV.[23] Numerous groups have reported significant changes in near-surface conductivity due to annealing in N_2 vs O_2 ambients,[1,4,22] which might be interpreted in terms of their respective influence on Ga and O vacancy concentrations.[21,25] In addition, Gao *et al.*[24] employed depth-resolved cathodoluminescence spectroscopy and surface photovoltage spectroscopy to examine the effects of near-surface oxygen plasma processing and irradiation damage on native point defects in β-Ga_2O_3 and they suggested that at least one oxygen vacancy-related and two gallium vacancy-related energy levels were involved, depending on sample processing conditions.[24]

Clearly, additional work is needed to understand the nature of processes underlying this behavior. A starting point is to isolate the physical damage effect from any chemical reaction mechanisms by exposing the Ga_2O_3 surface to Ar plasmas. In this paper, we present the results of a study of deep trap spectra, persistent photocapacitance, and minority carrier diffusion length in Ga_2O_3 films grown by halide vapor phase epitaxy (HVPE) and exposed to Ar plasmas. This results in an increase in the density of the E2* (Ec − 0.8 eV) and E3 (Ec − 1.05 eV) electron traps as well as deep acceptors with optical threshold for an ionization of ~2.3 eV and 3.1 eV.

EXPERIMENTAL

The samples were Si doped n-type β-Ga_2O_3 films grown by HVPE on heavily Sn-doped, n^+ β-Ga_2O_3 substrates prepared by edge-defined film-fed growth (EFG) by Tamura Corp. (Japan). Their orientation was (001). The donor concentration in the epitaxial layers was (2–4) × 10^{16} cm^{-3}, while the donor concentration in the substrates was (3–4) × 10^{18} cm^{-3}. The electron mobility in the epitaxial layers obtained from calibration samples grown on insulating substrates was ~300 cm^2 V^{-1} sec^{-1}. The thickness of the films was 10 μm; the substrates were 650-μm-thick. Figure 1 shows high resolution transmission electron microscope images of the near-surface region of the samples prior to plasma exposure (the left side shows the near surface region, and the right side shows the bulk region of the layer/substrate interface). There are no visible defects, and detailed characterization[26,27] has shown that these structures contain stacking faults with a density of 1.5 × 10^{10} cm^{-2} as well as threading screw dislocation densities of 30 cm^{-2} and basal dislocation densities of 20 cm^{-2}.

Full-area back Ohmic contacts were prepared by E-beam deposition of Ti/Au. Schottky diodes on the film surface were prepared by E-beam evaporation of Ni through a shadow mask.[28] Since there is no additional processing to this surface after plasma exposure, the I-Vs provide a sensitive measure of changes induced by the plasma process. The thickness of the Ni film was 20 nm, while the diameter of the Schottky diodes was 1 mm. Reference samples were not exposed to plasma treatment before Ni deposition. The other samples were subjected to Ar plasma at 300 °C for 2 min before deposition of Ni Schottky diodes. The inductively coupled plasma (ICP) reactor in which the plasma exposures occurred was operated at 40 mTorr, 2 MHz ICP power 500 W, and 13.56 MHz RF power of 140 W, corresponding to a self-bias of 330 V. The incident ion energy is then this self-bias minus the plasma potential of ~25 eV, i.e., the Ar ions were incident with ~305 eV energy. The incident ion energy correlates with the density of point defects created by the impinging ions. The O/Ga ratio in the plasma exposed region did not change from that in the reference material, at least to the sensitivity of Auger electron spectroscopy, but this does not exclude formation of native defects accessible only to optical and electrical characterization methods. Similarly, under these plasma exposure conditions, we would not expect to see crystal damage using TEM.[14,15]

Electrical characterization of the near-surface region of the samples consisted of capacitance vs frequency (C-f) at frequencies from 20 Hz to 1 MHz, capacitance-voltage (C-V) profiling at different frequencies in the dark and under illumination with high-power light emitting diodes with peak wavelengths ranging from 365 nm to 940 nm, current-voltage (I-V), microcathodoluminescence (MCL) at 300 K, and deep level transient spectroscopy (DLTS).[29] The diffusion length (L_d) of nonequilibrium charge carriers at room temperature was extracted from fitting the experimentally observed dependence of the collection efficiency of the electron beam induced

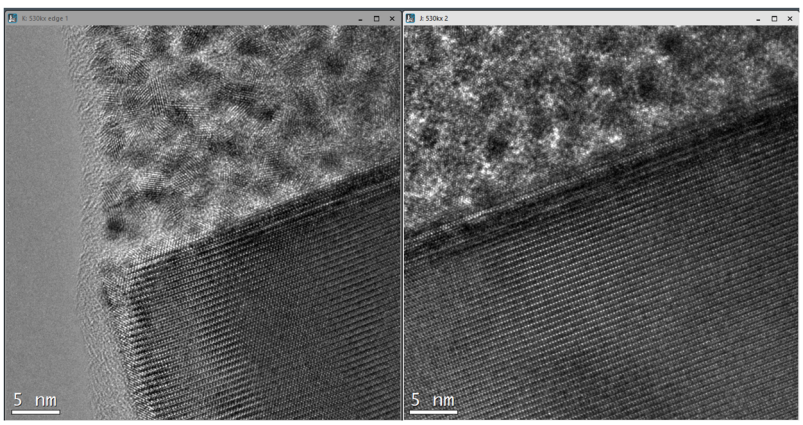

FIG. 1. High resolution TEM cross-sectional images from as-grown HVPE Ga_2O_3.

© Author(s) 2019

current (EBIC) on the probing electron beam energy of the scanning electron microscope (SEM).[30] Detailed descriptions of experimental setups can be found elsewhere.[31,32]

RESULTS AND DISCUSSION

The key outward differences between the reference samples and the Ar plasma treated samples are illustrated in Figs. 2(a)–2(c). As seen from Fig. 2(a), the capacitance at 0 V bias was considerably higher for the plasma exposed diodes. In $1/C^2$ vs voltage plots, presented in Fig. 2(b), the slopes of the dependences were close for both types of samples and corresponded to similar net donor concentrations N_d of 3.2×10^{16} cm^{-3} for reference samples and 4×10^{16} cm^{-3} for the Ar plasma samples. However, the voltage offset (V_{bi}) in the $1/C^2$ vs V plot was close to 1 V, corresponding to the usual Ni Schottky barrier height in (001) Ni diodes,[7,11] whereas for the Ar plasma exposed samples, V_{bi} was slightly negative, −0.019 V, which is a clear indication of the presence of a layer with high density of deep traps near the surface.[28] The barrier height determined from the temperature dependence of the forward current was ~0.9 eV (activation energy determined from the Arrhenius plot of forward current density at V = 0.5 V was 0.35 eV which gives the Schottky barrier height Φ_b of 0.85 eV when summed with qV, where q is the electronic charge[29]). The reverse current of the Ar plasma samples was much higher than for the reference samples, and the ideality factor in the forward I-V was 1.6 in the Ar plasma sample vs 1.02 for the reference sample [Fig. 2(c)].

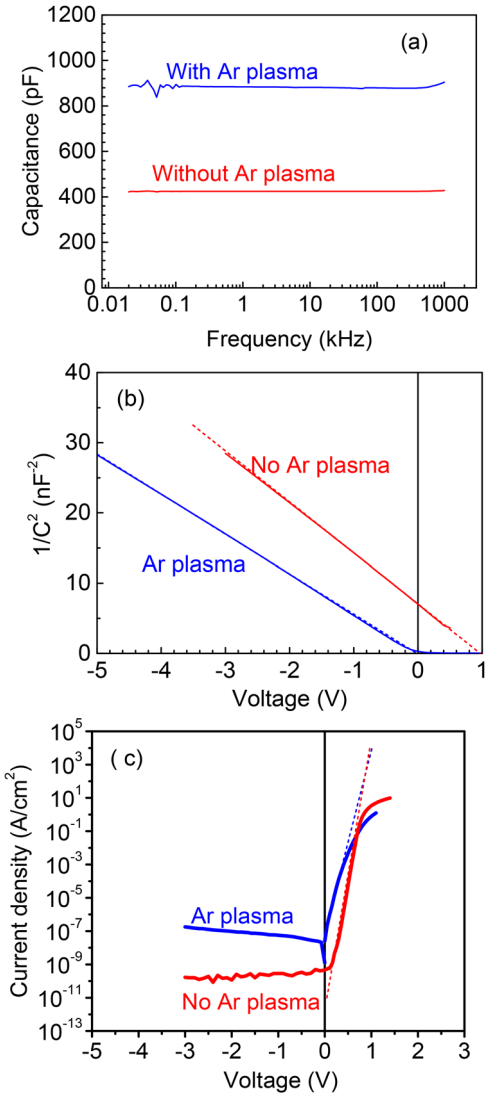

FIG. 2. (a) Room temperature C-f characteristics for reference (red line) and with Ar plasma treatment (blue line); (b) $1/C^2$ vs voltage plots with and without plasma treatment; (c) current-voltage characteristics.

The results in Fig. 2 are in qualitative agreement with observations reported for BCl_3/Ar plasma treatment under conditions for practical etch rates, although the changes in reverse current, voltage offset in C-V characteristics, and ideality factor increase were milder for the BCl_3/Ar plasma chemistry, as would be expected when switching from straight physical etching in Ar plasma to combined chemical plus physical etching in BCl_3/Ar plasmas.[14–17] This suggests that the underlying processes causing the observed changes are similar for both types of plasmas. The most important among them is the formation of deep electron and hole traps in the near surface region after the plasma treatment.

MCL spectra before and after Ar plasma treatment are shown in Fig. 3 for probe beam energies of 3 kV (a) or 10 kV (b). These correspond to approximate sampling depths of 0.3 and 2 μm, respectively. Note that the Ar plasma exposure leads to reduced intensity, which is more pronounced closer to the surface.

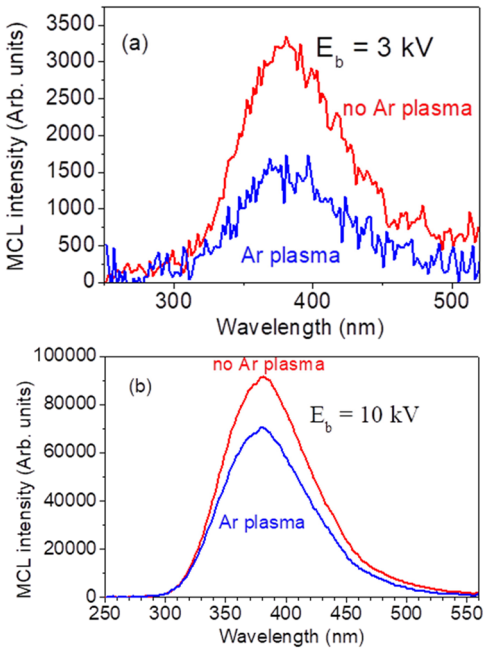

FIG. 3. MCL spectra at 300 K before and after Ar plasma treatment for (a) 3kV and (b) 10 kV probe beam energies.

© Author(s) 2019

To derive information on the deep acceptor states induced by plasma ion bombardment, C-V profiling under monochromatic illumination and photocapacitance spectra measurements were performed.[28,32] In the reference samples, no detectable signal could be observed either in photocapacitance spectra or in light C-V profiles, indicating low concentrations of deep traps in the lower part of the bandgap. This in agreement with previously reported results for similar HVPE films.[28,32] By sharp contrast, the Ar plasma samples showed measurable photocapacitance for photon energies above 2.3 eV [Fig. 4(a)]. For photon energies above 3.1 eV, the photocapacitance was persistent, i.e., kept almost constant, for a long period (>30 min) after illumination, even at room temperature.[28,32] This persistent signal could be strongly suppressed by application of forward bias pulses, as shown in Fig. 4(b). This process floods the space charge region (SCR) with electrons and eliminates the excess holes created by illumination on very deep hole traps with levels above ~E_v + 1.7 eV. Without this procedure, the traps can only be discharged by thermal excitation, which is very slow even at room temperature for these deep acceptors.[28,32] The spatial location of these traps could be determined by C-V profiling with monochromatic illumination. The results of these measurements are illustrated in Fig. 4(c). The signal in C-V profiles coming from deep acceptor centers is confined to the very near-surface part of the space charge region (SCR) with thickness below ~120 nm, although the penetration depth of respective photons is very much higher. Thus, the acceptors in question are created in the region of ~120 nm from the surface and are related to defects caused by Ar plasma damage. The centers with an optical threshold of ~2.3 eV are often observed in β-Ga_2O_3[33,34] and have been attributed to deep acceptors with optical ionization energy 2.1 eV. Their concentration increases with proton irradiation,[33,34] suggesting they involve native defects. The acceptors with an optical threshold of 3.1 eV have been associated with Ga vacancies.[28,32] An order of magnitude concentration can be derived by subtracting the concentration in the dark from the concentration on the plateau in the light C-V profiles in Fig. 4(c).

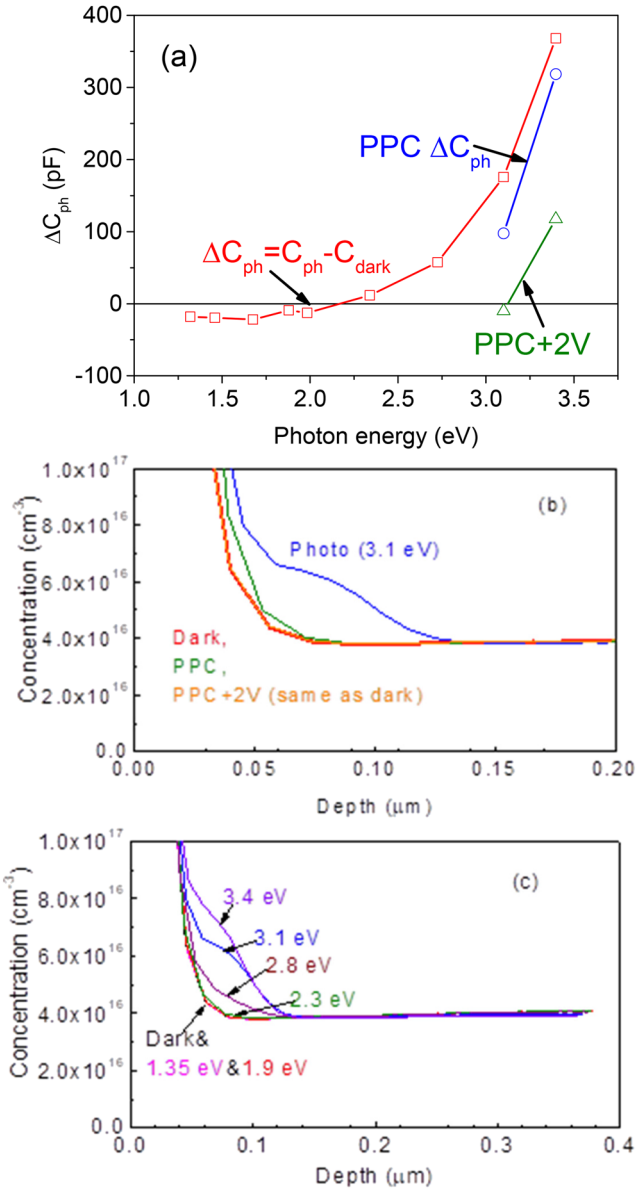

FIG. 4. (a) The spectral dependence of photocapacitance ΔC_{ph} [difference between capacitance under illumination C_{ph} and dark capacitance C_{dark} (open red squares)], persistent photocapacitance PPC ΔC_{ph}, and persistent photocapacitance after application of forward bias 2 V, PPC + 2 V; (b) concentration profiles in the dark, under illumination, and after additional application of forward bias of +2 V to quench the excess carriers; (c) concentration profiles in the dark and under illumination with photons of different energies.

DLTS spectra measurements performed on Ar plasma samples at different applied voltages and different heights of injection pulse provided information on the presence and distribution of deep electron traps. Figure 5(a) shows DLTS spectra measured with reverse bias −5 V pulsed to −3 V, with reverse bias −5 V pulsed to −1 V, and −1 V pulsed to 1 V. The y-axis of Fig. 5(a) gives the DLTS signal, ΔC/C, multiplied by $2N_d$ and divided by the spectrometer function F, $2N_d(\Delta C/C)/F$, where ΔC is the difference in transient capacitance values measured at time windows t_1 and t_2, C is the steady-state capacitance, and $F = \exp(-t_2/\tau) - \exp(-t_1/\tau)$, where $\tau = (t_2 - t_1)/\ln(t_2/t_1)$.[29] For temperatures corresponding to DLTS peaks, the spectra represented in these coordinates provide the concentrations of the respective deep traps without account for the so-called λ-correction that considers the change in the actual volume of SCR from which the DLTS signal is collected for different biases, trap levels, and Schottky barrier heights[28,29] [the convention in Fig. 5(a) is that positive peaks correspond to electron traps].

Essentially, the spectra in Fig. 5(a) provide such uncorrected information for probing different parts of the SCR, namely, at depth near 0.35 μm for the −5 V → −3 V bias/pulse sequence, surface region near 0.25 μm for −5 V → −1 V, and surface region near 0.1 μm for −1 V → 1 V. The location here was taken as the middle point between the SCR width corresponding to the applied steady-state bias and the bias during the injection pulse, as in double-correlation DLTS.[28,29] Due to the magnitude of the bias pulse, the position to which the concentration of deep traps is assigned is only approximate. However, qualitatively, it is obvious that their concentration becomes much higher as one approaches the surface.

© Author(s) 2019

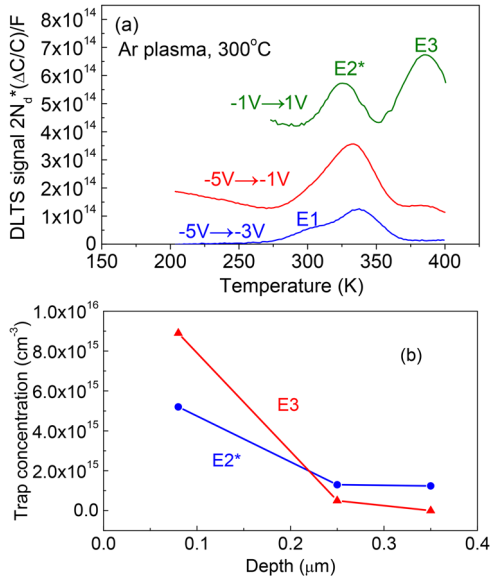

FIG. 5. (a) DLTS spectra measured for the Ar plasma treated sample under different bias/pulsing conditions (marked near each spectrum); the spectra are shown for time windows t_1/t_2 = 1.75 s/17.5 s, the pulse length of 3 s; (b) concentrations of deep traps after applying the λ-correction.

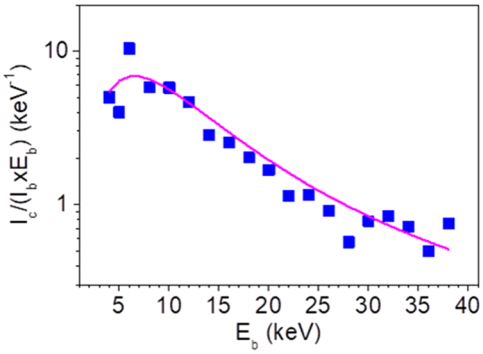

FIG. 6. EBIC collection efficiency vs beam energy E_b. The points are the experimental data, with the line fitting with L_d = 150 nm; I_c is the collected EBIC current and I_b is the probing beam current.

The "bulk" spectra obtained with the −5 V → −3 V sequence were characterized by the presence of two dominant deep traps with signatures similar to those of the E2* (E_c − 0.8 eV) and E3 (E_c − 1.05 eV) traps,[33–37] observed to also be effectively introduced by proton irradiation and most likely associated with complexes of native defects.[28,33–37] One can also see in the "bulk" spectrum in Fig. 5(a), a low energy shoulder corresponding to the deep trap with a level near E_c − 0.7 eV, most likely similar to the well-known E1 center.[33–35] This shoulder could not be resolved for the spectra taken nearer to the surface because it was masked by the increasing amplitude of the E2* peak. The two major E2* and E3 peak magnitudes in Fig. 5(a) rapidly increased nearer to the surface, and the ratio of magnitudes of the E3 to E2* peaks steadily decreased when moving away from the surface, suggesting the E3 traps become more abundant toward the surface. Figure 5(b) shows the concentrations of traps as a function of the distance from the surface when the λ-correction is taken into account. The density of electron traps strongly increases in the SCR region about 0.1 μm from the surface. In both the charge center concentration profiles measured in the dark and also the profiles under illumination in Fig. 4(b), there is a very strong buildup of the charged center concentration in the immediate vicinity of the surface. These centers do not produce any discernible peaks in DLTS and are most likely due to creation of conduction band tails by plasma damage induced defects at the surface. The increase in the structureless signal in DLTS spectra at low temperatures for the −1 V → 1 V bias/pulse sequence may be due to the contribution of these band tail states. The results are compared in Table I. Differences in the trap parameters for the two types of samples are attributable to experimental spread in DLTS measurements and net donor concentration and trap concentrations between different samples.

TABLE I. Deep trap levels and their concentration in reference and Ar plasma treated Ga_2O_3.

Sample	Trap level, E_a (eV)	Capture cross section, σ (cm^2)	Near-surface concentration (cm^{-3})	Bulk concentration (cm^{-3})	Minority carrier diffusion length (nm)
Reference	0.65	$4 \pm 1.5 \times 10^{-15}$	10^{13}	10^{13}	450
	0.8	$3 \pm 1.3 \times 10^{-14}$	3×10^{14}	3×10^{14}	
	1.05	$3 \pm 1.5 \times 10^{-14}$	5×10^{13}	5×10^{13}	
Ar plasma	0.7	$1.3 \pm 0.5 \times 10^{-14}$	Not detected	5.4×10^{13}	150
	0.8	$4 \pm 1.5 \times 10^{-14}$	5.2×10^{15}	4.2×10^{14}	
	1.05	$3 \pm 1.5 \times 10^{-14}$	8.9×10^{15}	3.2×10^{13}	
	2.3[a]		~2×10^{15}[b]	Not detected	
	3.1[a]		~4×10^{16}[b]	Not detected	

[a]Optical threshold in photocapacitance spectra.
[b]Estimated for the plateau in the light C-V profile with dark concentration subtracted.

© Author(s) 2019

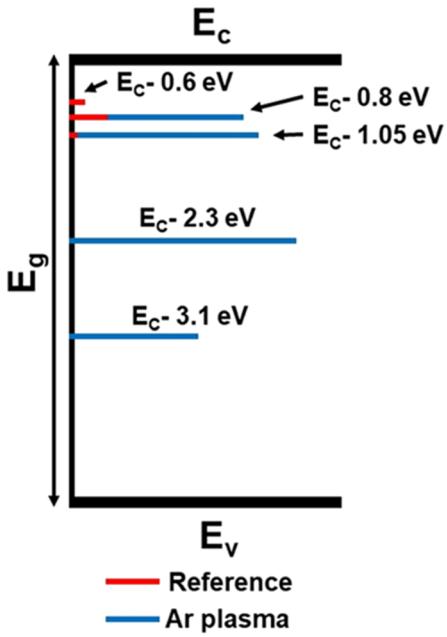

FIG. 7. Summary of energy levels and their concentration detected before and after Ar plasma exposure. The length of the bars represents the relative concentrations.

The diffusion length L_d estimated from EBIC collection efficiency dependence on SEM beam energy[30] decreased dramatically from 450 nm to 150 nm as a result of Ar plasma treatment, as shown in Fig. 6, for the plasma exposed samples. This is a consequence of formation of a damaged region with a high concentration of deep traps at the surface and consequent increased recombination rate within the space charge region. Figure 7 provides a summary of these trap states and their concentrations in the reference and plasma treated samples.

CONCLUSIONS

Exposure of HVPE β-Ga_2O_3 films to ICP Ar plasmas increases the density of deep electron traps E2* (E_c − 0.8 eV) and E3 (E_c − 1.05 eV) in the top ~100 nm of the films and creates in this region a high concentration of deep acceptors with optical threshold near 2.3 eV and 3.1 eV. These deep traps cause the apparent built-in voltage in C-V characteristics to strongly decrease from 1 V to −0.02 V and give rise to higher reverse leakage current and to an increase in the ideality factor in forward current. The introduction of these trap states also leads to a strong decrease in the diffusion length of nonequilibrium charge carriers from 450 nm in reference samples to 150 nm with Ar plasma exposure. Thus, the purely physical component of plasma exposure of β-(001) Ga_2O_3 degrades the near-surface electrical and transport properties, and annealing or short wet etch clean-up is needed to remove this surface damage. Some preliminary results on removing the plasma dry etch damage by 500 °C annealing have been reported elsewhere.[14,5] As for wet etching, it should be beneficial if properly optimized, although detailed studies have yet to be performed.

ACKNOWLEDGMENTS

The work at NUST MISiS was supported in part by the Ministry of Education and Science of the Russian Federation in the framework of Increase Competitiveness Program of NUST MISiS (No. K2-2017-068). The work at IMT RAS was supported by the State Task No. 075-00475-19-00. D.J.S. acknowledges the use of facilities in the John M. Cowley Center for High Resolution Electron Microscopy at Arizona State University. The work at UF was sponsored by the Department of the Defense, Defense Threat Reduction Agency, Grant No. HDTRA1-17-1-011, monitored by Jacob Calkins and by NSF No. DMR 1856662 (Tania Paskova).

REFERENCES

[1] A. Kuramata, K. Koshi, S. Watanabe, Y. Yamaoka, T. Masui, and S. Yamakoshi, Jpn. J. Appl. Phys., Part 1 **55**, 1202A2 (2016).
[2] S. Rafique, L. Han, A. T. Neal, S. Mou, M. J. Tadjer, R. H. French, and H. Zhao, Appl. Phys. Lett. **109**, 132103 (2016).
[3] H. von Wenckstern, Adv. Electron. Mater. **3**, 1600350 (2017).
[4] Z. Galazka, Semicond. Sci. Technol. **33**, 113001 (2018).
[5] M. J. Tadjer, L. E. Luna, E. Cleveland, K. D. Hobart, and F. J. Kub, ECS Trans. **85**, 21 (2018).
[6] S. I. Stepanov, V. I. Nikolaev, V. E. Bougrov, and A. E. Romanov, Rev. Adv. Mater. Sci. **44**, 63 (2016), available at http://www.ipme.ru/e-journals/RAMS/no_14416/06_14416_stepanov.pdf.
[7] S. J. Pearton, J. Yang, P. H. Cary, F. Ren, J. Kim, M. J. Tadjer, and M. A. Mastro, Appl. Phys. Rev. **5**, 011301 (2018).
[8] M. J. Tadjer, J. L. Lyons, N. Nepal, J. A. Freitas, A. D. Koehler, and G. M. Foster, ECS J. Solid State Sci. Technol. **8**, Q3187 (2019).
[9] M. H. Wong, K. Goto, Y. Morikawa, A. Kuramata, S. Yamakoshi, H. Murakami, Y. Kumagai, and M. Higashiwaki, Appl. Phys. Express **11**, 064102 (2018).
[10] M. A. Mastro, A. Kuramata, J. Calkins, J. Kim, F. Ren, and S. J. Pearton, ECS J. Solid State Sci. Technol. **6**, P356 (2017).
[11] S. J. Pearton, F. Ren, M. Tadjer, and J. Kim, J. Appl. Phys. **124**, 220901 (2018).
[12] Y. Zhang, Z. Xia, J. Mcglone, W. Sun, C. Joishi, A. R. Arehart, S. A. Ringel, and S. Rajan, IEEE Trans. Electron Devices **66**, 1574 (2019).
[13] S. Ohira and N. Arai, Phys. Status Solidi C **5**, 3166 (2008).
[14] J. Yang, S. Ahn, F. Ren, R. Khanna, K. Bevlin, D. Geerpuram, S. J. Pearton, and A. Kuramata, Appl. Phys. Lett. **110**, 142101 (2017).
[15] J. Yang, F. Ren, R. Khanna, K. Bevlin, D. Geerpuram, L.-C. Tung, J. Lin, H. Jiang, J. Lee, E. Flitsiyan, L. Chernyak, S. J. Pearton, and A. Kuramata, J. Vac. Sci. Technol., B: Nanotechnol. Microelectron.: Mater., Process., Meas., Phenom. **35**, 051201 (2017).
[16] J. E. Hogan, S. W. Kaun, E. Ahmadi, Y. Oshima, and J. S. Speck, Semicond. Sci. Technol. **31**, 065006 (2016).
[17] J. C. Yang, S. Ahn, F. Ren, S. J. Pearton, R. Khanna, K. Bevlin, D. Geerpuram, and A. Kuramata, J. Vac. Sci. Technol., B: Nanotechnol. Microelectron.: Mater., Process., Meas., Phenom. **35**, 031205 (2017).
[18] L. Zhang, A. Verma, H. G. Xing, and D. Jena, Jpn. J. Appl. Phys., Part 1 **56**, 030304 (2017).
[19] A. P. Shah and A. Bhattacharya, J. Vac. Sci. Technol., A **35**, 041301 (2017).
[20] J. Yang, Z. Sparks, F. Ren, S. J. Pearton, and M. Tadjer, J. Vac. Sci. Technol., B: Nanotechnol. Microelectron.: Mater., Process., Meas., Phenom. **36**, 061201 (2018).
[21] B. E. Kananen, L. E. Halliburton, K. T. Stevens, G. K. Foundos, and N. C. Giles, Appl. Phys. Lett. **110**, 202104 (2017).
[22] M. J. Tadjer, A. D. Koehler, J. A. Freitas, Jr., J. C. Gallagher, M. C. Specht, E. R. Glaser, K. D. Hobart, T. J. Anderson, F. J. Kub, Q. T. Thieu, K. Sasaki, D. Wakimoto, K. Goto, S. Watanabe, and A. Kuramata, Appl. Phys. Lett. **113**, 192102 (2018).
[23] M. J. Tadjer, N. A. Mahadik, J. A. Freitas, Jr., E. R. Glaser, A. Koehler, L. E. Luna, B. N. Feigelson, K. D. Hobart, F. J. Kub, and A. Kuramata, Proc. SPIE **10532**, 1053212 (2018).

© Author(s) 2019

[24]H. Gao, S. Muralidharan, N. Pronin, Md R. Karim, S. M. White, T. Asel, G. Foster, S. Krishnamoorthy, S. Rajan, L. R. Cao, M. Higashiwaki, H. von Wenckstern, M. Grundmann, H. Zhao, D. C. Look, and L. J. Brillson, Appl. Phys. Lett. **112**, 242102 (2018).
[25]J. B. Varley, J. R. Weber, A. Janotti, and C. G. Van de Walle, Appl. Phys. Lett. **97**, 142106 (2010).
[26]N. A. Mahadik, M. J. Tadjer, P. L. Bonanno, K. D. Hobart, R. E. Stahlbush, T. J. Anderson, and A. Kuramata, APL Mater. **7**, 022513 (2019).
[27]S. Masuya, K. Sasaki, A. Kuramata, S. Yamakoshi, O. Ueda, and M. Kasu, Jpn. J. Appl. Phys., Part 1 **58**, 055501 (2019).
[28]A. Y. Polyakov, N. B. Smirnov, I. V. Shchemerov, S. J. Pearton, F. Ren, A. V. Chernykh, P. B. Lagov, and T. V. Kulevoy, APL Mater. **6**, 096102 (2018).
[29]D. K. Schroeder, *Semiconductor Material and Device Characterization* (John Wiley & Sons, New York, 1990), p. 587.
[30]E. B. Yakimov, A. Y. Polyakov, N. B. Smirnov, I. V. Shchemerov, J. Yang, F. Ren, G. Yang, J. Kim, and S. J. Pearton, J. Appl. Phys. **123**, 185704 (2018).
[31]A. Y. Polyakov, N. B. Smirnov, In-H. Lee, and S. J. Pearton, J. Vac. Sci. Technol., B: Nanotechnol. Microelectron.: Mater., Process., Meas., Phenom. **33**, 061203 (2015).
[32]A. Y. Polyakov, N. B. Smirnov, I. V. Shchemerov, E. B. Yakimov, S. J. Pearton, C. Fares, J. Yang, F. Ren, J. Kim, P. B. Lagov, V. S. Stolbunov, and A. Kochkova, Appl. Phys. Lett. **113**, 092102 (2018).
[33]M. E. Ingebrigtsen, J. B. Varley, A. Yu. Kuznetsov, B. G. Svensson, G. Alfieri, A. Mihaila, U. Badstübner, and L. Vines, Appl. Phys. Lett. **112**, 042104 (2018).
[34]Z. Zhang, E. Farzana, A. R. Arehart, and S. A. Ringel, Appl. Phys. Lett. **108**, 052105 (2016).
[35]K. Irmscher, Z. Galazka, M. Pietsch, R. Uecker, and R. Fornari, J. Appl. Phys. **110**, 063720 (2011).
[36]Y. Nakano, ECS J. Solid State Sci. Technol. **6**, P615 (2017).
[37]E. Farzana, E. Ahmadi, J. S. Speck, A. R. Arehart, and S. A. Ringel, J. Appl. Phys. **123**, 161410 (2018).

© Author(s) 2019